PREPRINT UCRL-78433

Conf-761108--4

Lawrence Livermore Laboratory

ZONE PLATE CODED IMAGING OF LASER COMPRESSED TARGETS

N. M. Ceglio and E. V. George, MIT

K. M. Brooks, K. R. Manes, L. W. Coleman, and H. G. Ahlstrom

September, 1976

This paper was prepared for presentation at the American Physical Society, 1976 Annual Meeting of the Division of Plasma Physics, November 15-19, 1976 San Francisco, CA

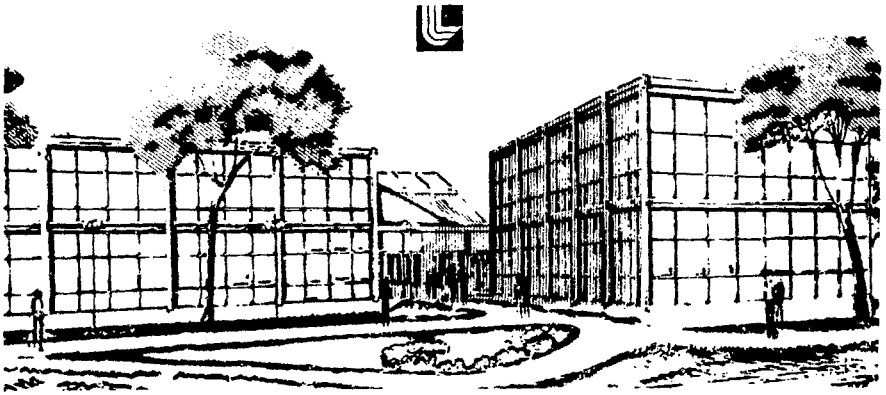

ZONE PLATE CODED IMAGING OF LASER COMPRESSED TARGETS*

N. M. Ceglio and E. V. George, MIT
K. M. Brooks, K. R. Manes, L. W. Coleman, and H. G. Ahlstrom
Lawrence Livermore Laboratory, University of California
Livermore, California 94550

Abstract

The first successful demonstration of high resolution, tomographic imaging of a laboratory plasma using coded imaging techniques is reported. ZPCI has been used to image the x-ray emission from laser compressed DT filled microballoons. The zone plate camera viewed an x-ray spectral window extending from below 2 kev to above 6 kev. It exhibited a resolution ~ 8 μm, a magnification factor ~ 13, and subtended a radiation collection solid angle at the target $\sim 10^{-}$ sr. X-ray images using ZPCI were compared with those taken using a grazing incidence reflection x-ray microscope. The agreement was excellent. In addition, the zone plate camera produced tomographic images. The nominal tomographic resolution was ~ 75 μm. This allowed three dimensional viewing of target emission from a single shot in planar "slices". In addition to its tomographic capability, the great advantage of the coded imaging technique lies in its applicability to hard (> 10 kev) x-ray and charged particle imaging. Experiments involving coded imaging of the suprathermal x-ray and high energy alpha particle emission from laser compressed microballoon targets are discussed.

Introduction

Coded imaging techniques have been used in astronomy[1, 2] and nuclear medicine[3, 4] for imaging short wavelength radiations not easily focused using conventional reflection, refraction or diffraction techniques. The appropriateness of a particular coded imaging technique, Zone Plate Coded Imaging (ZPCI), for x-ray and charged particle imaging of laser produced plasmas was recently suggested.[5] This paper reports the first successful application of ZPCI to high resolution (~ 8 μm), tomographic (~ 74 μm tomographic resolution) imaging of the x-ray emission from laser compressed targets. In addition, experiments involving Zone Plate Coded Imaging of the suprathermal x-ray and high energy alpha particle emission from laser compressed microspheres are proposed and discussed.

X-ray Imaging (2 - 6 kev):

The experiments reported here were conducted using the Cyclops[6] laser-target irradiation facility at Lawrence Livermore Laboratory. The targets used were deuterium-tritium filled glass microballoons[7], typically 100 μm in diameter. The target was compressed by simultaneous, two sided irradiation by an intense neodymium laser pulse. X-ray emission from the compressed target was imaged using ZPCI, and the images compared with those of a well established diagnostic - the grazing incidence reflection x-ray microscope.[8]

*Work performed under the auspices of the U. S. Energy Research and Development Administration under contract No. W-7405-Eng-48.

The theory and details of laboratory implementation of the ZPCI technique are discussed elsewhere.[9-12] The zone plate camera used in these experiments had a coded aperture of 100 zones with a smallest zone width $\Delta r = 5.3$ μm. The zone plate material was gold, 1.4 μm thick. Details for zone plate fabrication are provided elsewhere.[13] The camera had a planar resolution of 8 μm, and a tomographic resolution of approximately 74 μm. It viewed the plasma in an x-ray spectral window extending from below 2 Å to above 6 Å. The long wavelength recording was limited by a 125 μm thick Be filter, while the short wavelength limit was set in this experiment by the rapid decay of x-ray emission in this spectral region. The imaging geometry was characterized by the following parameters: $s_2/s_1 \simeq 16$ (± 10%); $s_1 \simeq 1$ cm (± 10%); solid angle subtended by coded aperture $\simeq 1.75 \times 10^{-2}$ sr. The parameters s_1, s_2 are the source to zone plate and zone plate to coded image (shadowgraph) distances respectively.

Typical ZPCI results are shown in Figures 1 and 2. The data in Figures 1 and 2 are organized in the following way. The coded image of the x-ray source distribution is presented in (a); (b) is a two dimensional isodensity contour map of the image reconstructed from (a); (c) is a quasi-three dimensional representation of the microdensitometer data of (b); the vertical scale of (c) represents image density. The figures are scaled in image dimensions. The magnification factor for the data of Figure 1 is 12.8 and for Figure 2 is 13.4. In the experiment recorded in Figure 1 the laser energy on target was 33 joules in a pulse of 46 psec (FWHM) and significant target compression was achieved. There is excellent agreement between Figure 1 and x-ray microscope images of the same shot.[10] Figure 2 shows image data for a low energy (5 joules in 53 psec) laser shot in which no target compression occurred. The x-ray flux from this poorly irradiated target was insufficient to yield x-ray microscope images. Figure 2 is, thereby, a direct illustration of the (S/N) and sensitivity advantage of the zone plate camera due to its large solid angle for radiation collection.[14]

Tomographic data from the low energy (no compression) shot are presented in Figure 3. Shown are isodensity contour maps for reconstructed images viewed in three separate reconstruction planes. Figure 3(a) is representative of the source plane at the geometrical center of the plasma shell, Figure 3 (b) is an image of the source plane a distance 37 μm behind (viewed from the zone plate camera) the central plane, and Figure 3(c) is an image of the source plane, a distance 74 μm behind the central plane.[15] Due to the relatively large value of the tomographic resolution limit (i.e., $\Delta = 74$ μm) in this experiment, the amount of significant physical information which can be extracted from the data of Figure 3 is small. One should note, however, the migration of the region of peak density in the contour pattern on the left. In Figure 3(a) the peak density region is approximately 23 μm above the equatorial plane of the plasma shell. It migrates down toward the equatorial plane as we view rear sections of the plasma shell until in Figure 3(c) it is only 4 μm above the equatorial plane.

X-ray Imaging (8 - 20 kev):

The x-ray emission spectrum from laser compressed microspheres is known to exhibit a high energy tail (≃ 10-88 kev). Typical x-ray emission spectra from experiments conducted using the (a) Janus and (b) Argus laser irradiation facilities are shown in Figures 4(a) and 4(b).[16] The targets were deuterium-tritium filled glass microballoons.

Suprathermal x-ray emission can be imaged using ZPCI techniques. Free standing zone plates adequate for such imaging experiments have recently been fabricated.[11, 13] Zone plate characteristics and imaging capabilities for zone plates of 100 and 240 zones are listed in Table I. Long wavelength recording will be limited by a 25 μm thick Mo filter, while the short wavelength limit will be set by transmission of source radiation through the solid zones of the coded aperture during image encoding. Figure 5 shows plots of the fractional transmission versus x-ray wavelength for the 25 μm Mo foil and the 5.0 μm thick gold zones.[17] Figures 6(a) and 6(b) show the x-ray spectra transmitted through the 25 μm Mo foil. It is clear from Figures 5, 6(a) and 6(b) that x-rays below 8 kev do not make significant contribution to the coded image because of strong attenuation by the Mo foil. On the other hand, x-rays of energy above 20 kev yield coded images of very poor contrast so that they cannot make significant contributions to the reconstructed images.[10-13]

α-Particle Imaging:

High resolution imaging of the region of thermonuclear burn in a laser compressed target is a high priority goal of the laser fusion program at Lawrence Livermore Laboratory. Attempts at imaging the α-particle emission from compressed deuterium-tritium targets are complicated by the low α-particle flux (on the order of 5×10^8 α's per shot using the Argus facility) and the relatively high background radiation flux (typically 5 joules of x-ray and 35 joules of heavy ion (silicon, oxygen) emission per shot using the Argus facility).

α-particle emission from laser compressed targets can be imaged using ZPCI techniques. Zone plates to be used in such experiments should be free standing and have a thickness $\gtrsim 5$ μm. Zone plates should not be substrate supported because scattering of the α's in the substrate material can cause blurring of the coded image and impair resolution.[18] Although scattering of the α's in the substrate material is small, the displacement of the scattered α's in the coded image is amplified by the large ($\lesssim 10$ cm) values of s_2 (distance from zone plate to coded image). A zone plate thickness $\gtrsim 5$ μm (gold) is required to stop the 3.5 Mev α's.[19] Zone plate characteristics and α-particle imaging capabilities for free standing structures of 100 and 240 zones are listed in Table I.

Discrimination between α's and heavier ions may be achieved using a thin absorber foil in intimate[20] contact with the recording film in the shadowgraph plane. The absorber foil will selectively absorb the heavy ions (ion range $\sim 1/Z^2$) while allowing the α's to pass through with only a moderate energy decrease. Close contact between the absorber foil and the recording film is necessary to minimize the effects of α-particle scattering in the foil.

Discrimination between α's and x-rays can be achieved by selection of an appropriate shadowgraph (coded image) recording medium. Photographic emulsions are much more sensitive to α radiation than x-rays because of the higher specific energy deposition (erg/cm) for heavy charged particles in the photographic medium. In addition, various thin sheet polymers (e.g.: cellulose nitrate) will record α-particle tracks while remaining insensitive to x-rays.

Conclusion

The viability of ZPCI techniques has been demonstrated for high resolution imaging of the moderate energy (2-6 kev) x-ray emission from laser compressed targets. It is shown that these techniques can also be used to image the supra-thermal (8-20 kev) x-ray emission and α-particle emission from such targets.

References

1. L. Mertz and N. O. Young, Proc. Int. Conf. on Opt. Instr., London (1961) p. 305.
2. R. H. Dicke, Astrophys. J. 153, L101 (1968).
3. W. L. Rogers, L. W. Jones, W. H. Beierwaltes, Optc. Eng., 12,13 (1973).
4. H. L. Caulfield and A. D. Williams, Opt. Eng. 12, 3 (1973).
5. N. M. Ceglio and E. V. George, Bull. Am. Phys. Soc. 20, 1350 (1975).
6. Lawrence Livermore Laboratory, Laser Program Annual Report - 1974, UCRL 50021-74, p. 42, March 1975.
7. Ibid, p. 365.
8. F. Seward, J. Dent, M. Boyle, L. Kappel, T. Harper, P. Stoering and A. Toor, Rev. Sci. Instr. 47, 464 (1976).
9. N. M. Ceglio, App. Phys. Lett, submitted for publication
10. N. M. Ceglio, Massachusetts Institute of Technology, Ph.D. Thesis, August 1976.
11. Henry I. Smith and N. M. Ceglio, Bull. Am. Phys. Soc. 21 (Oct. 1976).
12. N. M. Ceglio, "Zone Plate Coded Imaging - A New Plasma Diagnostic", to be submitted for publication.
13. N. M. Ceglio and H. I. Smith, "Fabrication of Micro Fresnel Zone Plates for Coded Imaging Applications", unpublished.
14. X-ray microscopes, on the other hand do not require reconstruction and are capable of combining micron spatial resolution with a large object distance. The latter is a significant attribute for future laser fusion studies where unabsorbed laser light, reaction products and general target debris may be destructive for close-in diagnostic devices.
15. In practical terms the image viewed in a given reconstruction plane is representative of the radiation contributions from a slice of the source distribution approximately Δ thick.
16. These spectra are provided courtesy of H. Kornblum, Lawrence Livermore Laboratory.
17. H. M. Stainer, ed., X-Ray Mass Absorption Coefficients, U. S. Department of the Interior, Bureau of Mines (1963).
18. E. Fermi, Nuclear Physics (University of Chicago Press, 1950), Ch. 2.
19. R. D. Evans, The Atomic Nucleus (McGraw-Hill, 1955) Ch. 22.
20. Protection of the film surface can be accomplished by using a thin (1/8-1/4 mil) Kapton film layer between the absorber foil and the recording film.

Acknowledgments

The authors wish to thank D. T. Attwood for his assistance. In addition, we wish to recognize the efforts and cooperation of M. Boyle, J. Houghton, W. M. Mulligan, H. I. Smith, H. Kornblum, V. Slivinsky and A. H. Firester.

Table I

Catalogue of Zone Plate Characteristics and Imaging Capabilities[10-13]

Characteristics / Capabilities	Type I	Type II
N	100	240
Δr	5.3 μm	5.3 μm
δ	≈ 7.7 μm	≈ 7.7 μm
$\Delta_{(a)}$	≈ 75 μm	≈ 31 μm
$\Delta_{(b)}$	≈ 38 μm	≈ 16 μm
$\Delta_{(c)}$	≈ 19 μm	≈ 8 μm
$\Omega_{(a)}$	1.75×10^{-2} sr	9.70×10^{-2} sr
$\Omega_{(b)}$	6.83×10^{-2} sr	3.42×10^{-2} sr
$\Omega_{(c)}$	2.49×10^{-1} sr	9.40×10^{-1} sr
R	≈ 34	≈ 81
$\alpha\text{flux}^{*}_{(c)}$	$\approx 2 \times 10^{6}$ cm^{-2}	$\approx 2 \times 10^{6}$ cm^{-2}

where

N = total number of zones
Δr = width of the outermost zone
t = zone plate thickness ≈ 5 μm
δ = planar resolution of zone plate camera
Δ = tomographic resolution of zone plate camera
Ω = solid angle for radiation collection
R = anticipated (S/N) enhancement factor for the zone plate camera relative to an equivalent pinhole camera

subscript (a) implies the assumption $S_1 = 1$ cm $S_2 \gg S_1$
(b) implies the assumption $S_1 = .5$ cm $S_2 \gg S_1$
(c) implies the assumption $S_1 = .25$ cm $S_2 \gg 1$

*The calculation of the time integrated α-particle flux at the coded image plane assumes a total emission of 2×10^{8} α particles and an image magnification factor of 10.

Figure Captions

Figure 1. ZPCI data for a laser compressed target. The figure is scaled in image dimensions. The magnification factor is 12.8.

(a) Coded image
(b) Isodensity contour map of the reconstructed image. The density contour interval is .05.
(c) Quasi-three dimensional representation of the microdensitometer data of (b). Image density, $\mathcal{D}$, is represented vertically.

Figure 2. ZPCI data for a laser irradiated target exhibiting no compression. The figure is scaled in image dimensions. The magnification factor is 13.4.

(a) Coded image
(b) Isodensity contour map of the reconstructed image. The density contour interval is .1.
(c) Quasi-three dimensional representation of the microdensitometer data of (b). Image density, $\mathcal{D}$, is represented vertically.

Figure 3. Tomographic data for a laser irradiated target exhibiting no compression. Isodensity contour maps are shown. The density contour interval is .1 in all cases. The figures are scaled in image dimensions. The magnification factor is 13.4.

(a) Reconstructed image of the source "plane" at the geometrical center of the plasma shell.
(b) Reconstructed image of the source "plane" a distance 37 μm behind the central plane.
(c) Reconstructed image of the source "plane" a distance 74 μm behind the central plane.

Figure 4. Typical x-ray emission spectra from experiments conducted using the (a) Janus and (b) Argus laser irradiation facilities are shown.

Figure 5. Plotted are curves of the fractional transmission versus x-ray wavelength for the 25 μm Mo foil (solid line) and the 5.0 μm thick gold zones (broken line).

Figure 6. Plotted are the transmitted x-ray spectra through 25 μm Mo foil for typical shots on the (a) Janus and (b) Argus facilities.

(a)

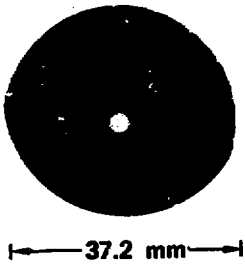

(b)

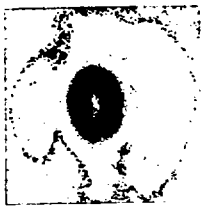

(c)

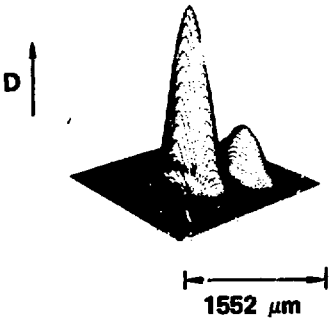

Figure

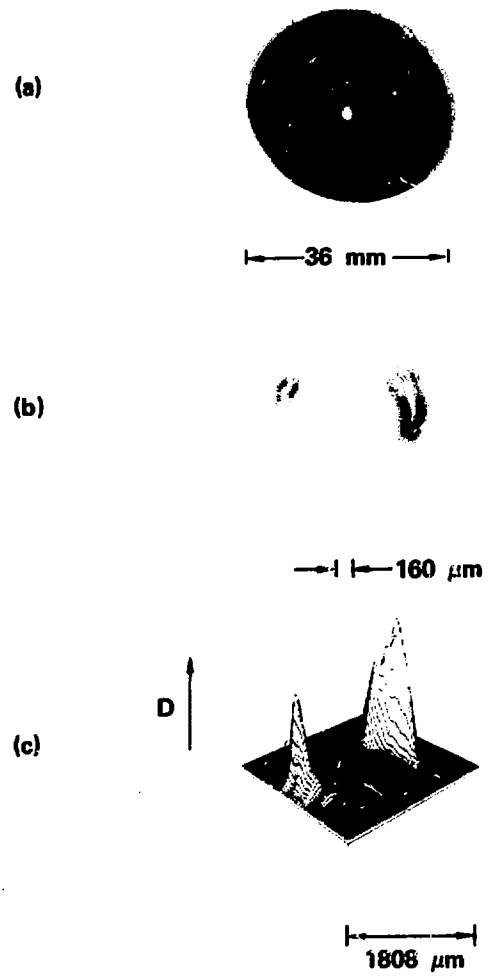

Figure 2

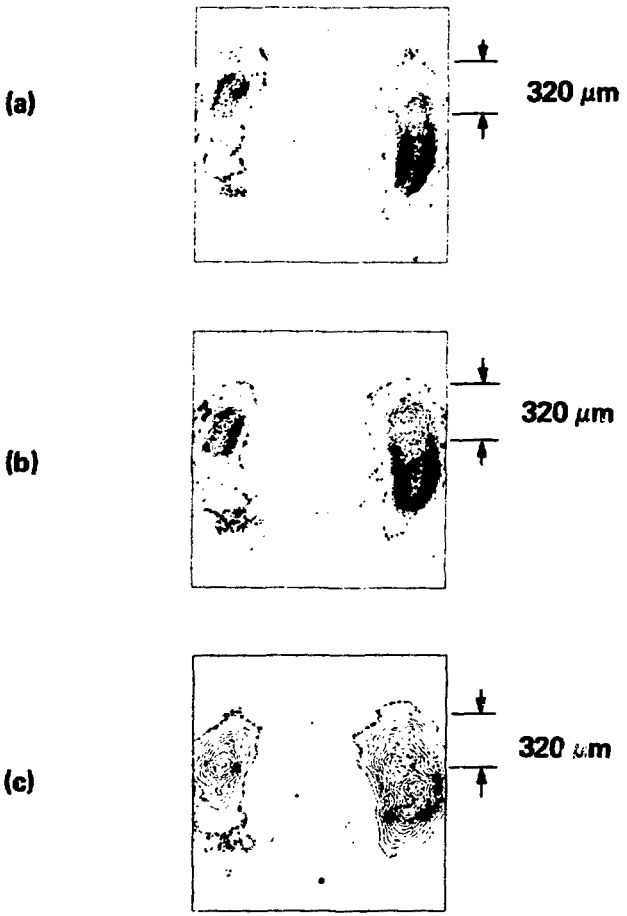

Figure 3

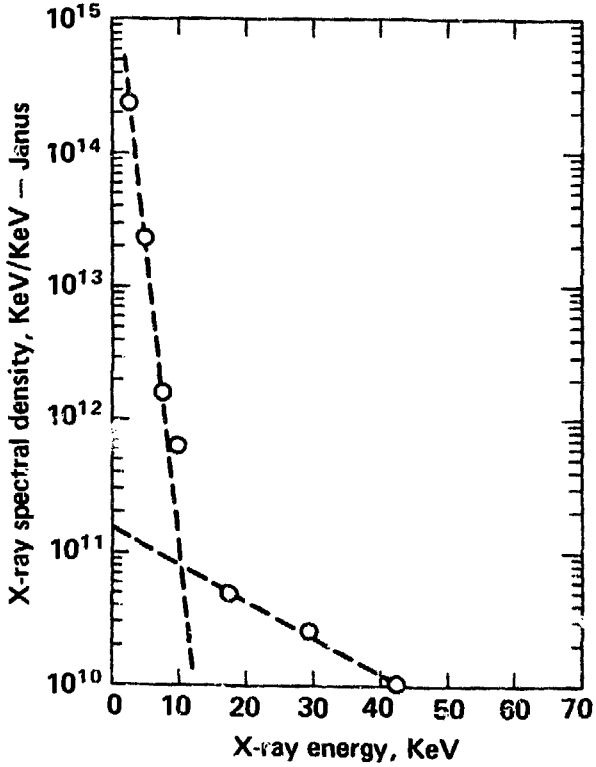
X-ray spectral density, KeV/KeV — Janus
10^{15}
10^{14}
10^{13}
10^{12}
10^{11}
10^{10}
0
10
20
30
40
50
60
70
X-ray energy, KeV

Figure 4(a)

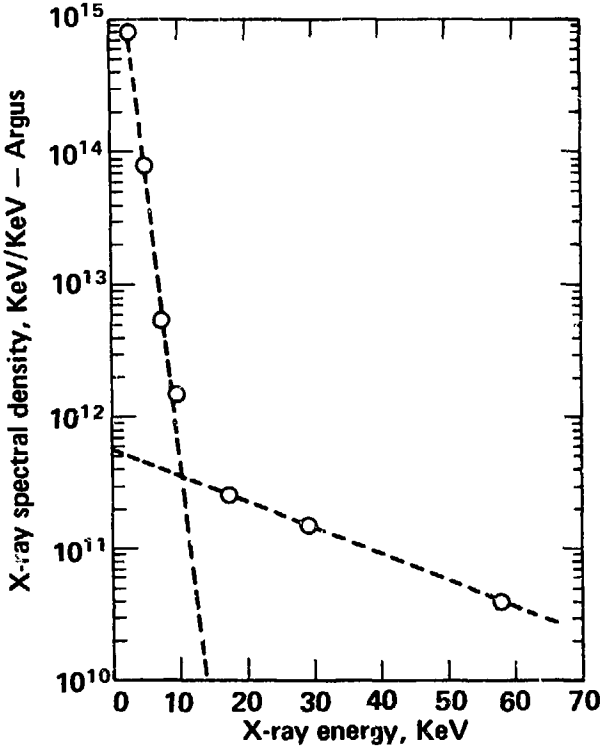
X-ray spectral density, KeV/KeV – Argus
10^{15}
10^{14}
10^{13}
10^{12}
10^{11}
10^{10}
0
10
20
30
40
50
60
70
X-ray energy, KeV

Figure 4(b)

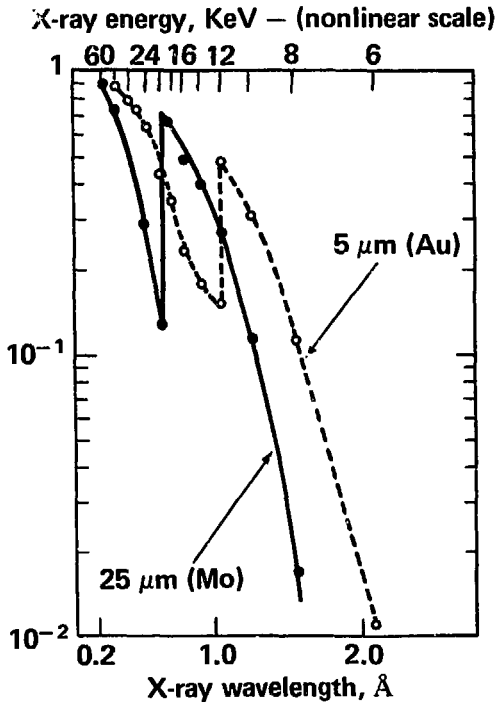
X-ray energy, KeV — (nonlinear scale)
1
60 24 16 12 8 6
5 μm (Au)
10^{-1}
25 μm (Mo)
10^{-2}
0.2
1.0
2.0
X-ray wavelength, Å

Figure 5

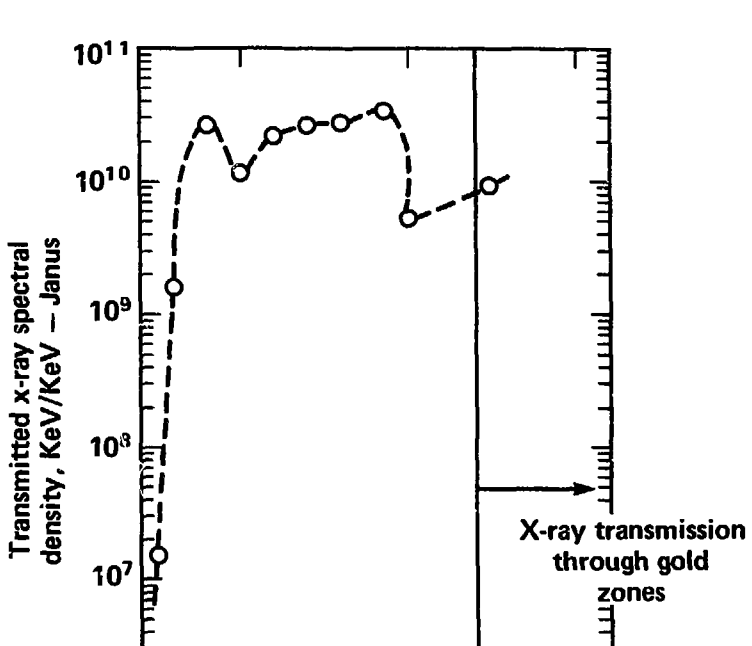
Transmitted x-ray spectral density, KeV/KeV – Janus
10^{11}
10^{10}
10^{9}
10^{8}
10^{7}
10^{6}
4
10
20
30
X-ray energy, KeV
X-ray transmission through gold zones

Figure 6(a)

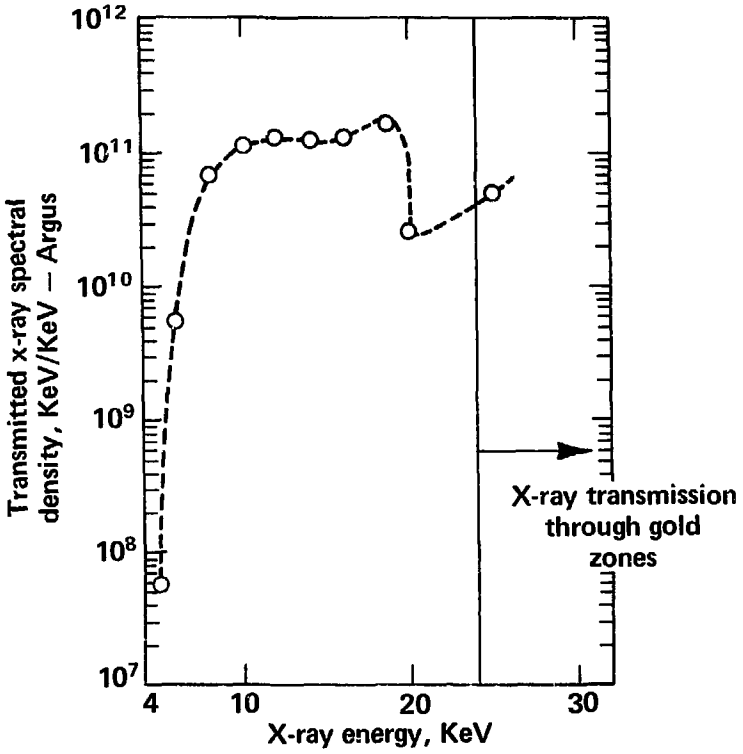
10^{12}
10^{11}
10^{10}
10^{9}
10^{8}
10^{7}
Transmitted x-ray spectral density, KeV/KeV — Argus
4
10
20
30
X-ray energy, KeV
X-ray transmission through gold zones

Figure 6(b)